Int. J. Multiphase Flow, Vol. 1, pp. 555–572. Pergamon Press, 1974. Printed in Great Britain.

DIRECT CONTACT HEAT EXCHANGERS: COMPARISON OF COUNTER AND CO-CURRENT CONDENSERS*

SAMUEL SIDEMAN and DAVID MOALEM**

Department of Chemical Engineering, Technion—Israel Institute of Technology, Haifa (Israel)

(Received January 7, 1974)

Summary

Contact condensers exhibit high heat transfer rates, compactness, absence of scale and can be operated even at very low temperature driving forces. A technique successfully utilized earlier by the authors to predict the condensation rate — and height — of a single bubble train, is extended here to predict the condenser height in counter and co-current multi-bubble systems. This approach makes it possible to distinguish the effect of the bubbles' spatial density, *i.e.* effects of bubble frequency and horizontal spacing.

Introduction

Direct contact exchangers, in which heat is transferred between a volatile dispersed fluid and an immiscible or miscible liquid media, are extremely efficient. The present work, motivated by the quest for more efficient 3-phase exchangers as well as for additional insight into the transfer mechanism, deals with condensation of gravity-driven vapor bubbles and supplements our earlier analysis of a counter current exchanger [1].

A lumped-parameter approach yields, via an energy balance over the continuous, steady state column, the inlet and outlet conditions. The height of the (liquid) column, which corresponds to the time required for 99% of total possible condensation, depends on the transfer rates. These, in turn, depend on interaction between the bubbles (frequency F and number of nozzles n), and on the flow and temperature fields.

Simultaneous numerical solution of the interrelated energy and momentum equations, while possible for a single train [2], is obviously out of the question for a multi-train system. Hence, an approximate analytical solution, an extension of the one successfully utilized in single [3] and multi-train [1] studies, is generalized here. In essence, we deal with the effects of the rise velocity and temperature field under various operating conditions on the collapse history of a single bubble in a multi-bubble system. Use is made of

*Presented at the Fourth International Symposium on Fresh Water from the Sea, Heidelberg, September, 1973.

**Present address: School of Engineering, University of Tel-Aviv, Ramat Aviv, Israel.

the quasi-steady state solution for a single bubble in potential, or modified-potential, flow field [4]. In addition to its simplicity, this approach leads to a general solution, encompassing single and two-component systems (single-phase and two-phase bubbles, respectively) and including non-condensables, whether homogeneously or non-homogeneously distributed [5] inside the bubble.

The general collapse equations

For a single bubble rising freely in an unconfined liquid column at a velocity U_∞, the average heat flux in a potential flow field under quasi-steady state conditions (Pe > 1000, and $\partial R/\partial t << U_\infty$) is given by [3, 6]:

$$q = k \frac{(T - T_\infty)}{\sqrt{\pi}} \frac{1}{R} (2RU_\infty/\alpha)^{1/2} \tag{1}$$

where $T = T^*$ for pure vapor and $T = T_w$, the wall temperature, in the presence of inerts. $T_w = T^*$ when the initial molar concentration of the inerts $Y_0 = 0$. Equation (1) with the energy balance at wall of the collapsing bubble, *i.e.* $(-\lambda \dot{R} \rho_v)$ yields:

$$R = -\frac{k\Delta T}{\rho_v \lambda} \left(\frac{2U_\infty}{\pi\alpha R}\right)^{1/2}; \quad \Delta T = T_w - T_\infty \tag{2}$$

where R is the instantaneous radius. Defining

$$\theta_w \equiv (T_w - T_\infty)/(T^* - T_\infty); \quad \tau \equiv \text{Ja Pe}^{1/2} \text{ Fo}; \quad \beta = R/R_0$$

$$\text{Ja} = \rho C_p (T^* - T_\infty)/\lambda \rho_v; \quad \text{Pe} = 2R_0 U_\infty/\alpha; \quad \text{Fo} = t\alpha/R_0^2$$

Eqn. (2) reduces to

$$\dot{\beta} = -\frac{1}{\sqrt{\pi}} \frac{1}{\beta^{1/2}} \theta_w; \quad \beta = 1 \text{ at } \tau = 0 \tag{3}$$

The application of eqn. (2), or (3), for the case at hand requires re-defining the operating parameters in accordance with the conditions prevailing in a multi-bubble column. Thus, U_∞^M replaces U_∞ and T_∞^M replaces T_∞, where the superscript M denotes the bubble-density dependent parameters. However, for ease of comparison with single bubble studies, the Ja and Pe numbers are left unchanged as defined above.

The modified eqn. (3) now reads:

$$-\dot{\beta}^M = -\left(\frac{d\beta}{d\tau}\right)^M = \frac{1}{\sqrt{\pi}} (U_\infty^M/U_\infty)^{1/2} \theta_w^M \frac{1}{\beta^{1/2}} \tag{4}$$

where in terms of the local field temperature T_∞^M or the local temperature increase $T_\infty^M - T_\infty = \delta T^M$

$$\theta_w^M \equiv \frac{\Delta T^M}{\Delta T^*} = \frac{T_w - T_\infty^M}{T^* - T_\infty} = \theta_w - \frac{\delta T^M}{T^* - T_\infty} \equiv \theta_w - \delta\theta^M \tag{5}$$

Note that θ_w is the dimensionless temperature driving force for a single bubble system, and $\delta\theta^M$ represents the fractional decrease of the temperature driving force affected by the multi-bubble system. Introducing K_v, the velocity factor by which the potential flow solution for flow around a sphere is "transformed" to yield the average heat flux that would be obtained in a viscous flow field [4, 7]:

$$K_v = 0.25\ \mathrm{Pr}^{-1/3} \tag{6}$$

For a two-phase bubble (for a single phase bubble $K_v = 1$), and defining

$K = (K_v/\pi)^{1/2}$; $A = (U_\infty^M/U_\infty)^{1/2}$; $B = A\delta\theta^M$

eqn. (4) reduces to

$$-\frac{1}{K}\left[\frac{d\beta}{d\tau}\right]^M = A(\theta_w - \delta\theta^M)\frac{1}{\beta^{1/2}} = \frac{A\theta_w}{\beta^{1/2}} - \frac{B}{\beta^{1/2}} \tag{7}$$

The solution of eqn. (7) depends on the relation between θ_w and β, which for a homogeneous distribution of the inerts within the bubble is given by [7]:

$$\theta_w = \frac{\beta^3 - \beta_f^3}{\beta^3 - 1/G^*}\ ;\ \beta_f = R_f/R_0 \quad G^* = \rho_L/\rho_v \tag{8}$$

The term $1/G^*$ in eqn. (8) is due to the condensed liquid which accumulates in the "two-phase" bubble (say pentane condensing in water) in contrast to the single-phase bubble (say pentane condensing in pentane). In the absence of noncondensables $\beta_f = 0$ for the single-phase bubble and $\beta_f = G^{*-1/3}$ for the two-phase bubble. The dependence of β_f on Y_0, the initial mole fraction of inerts, is given in [7]. The relation between θ_w, β and Y_0 for nonhomogeneous distribution of the inerts within the bubble is given in ref. [5].

The time-dependent radius

For a pure vapor, $T_w = T^*$ and $\theta_w = 1$. Equation (7) reduces to:

$$-\frac{1}{K(A-B)}\left(\frac{d\beta}{d\tau}\right) = \frac{1}{\beta^{1/2}}\ ;\ \beta = 1 \text{ at } \tau = 0 \tag{9}$$

Integration of eqn. (9) yields:

$$\tau_0^M = \frac{1}{A-B}\left(\frac{\pi}{K_V}\right)^{0.5}\frac{2}{3}(1-\beta^{3/2}) \equiv \frac{1}{A-B}\ \tau_0 \tag{10}$$

where τ_0 is the dimensionless time variable for (pure) single bubble condensation, directly obtainable by integrating eqn. (2). Obviously, for a single bubble $A = (U_\infty^M/U_\infty)^{1/2} = 1$, $B = 0$ (since $\delta\theta^M = 0$) and $\tau_0^M = \tau_0$.

For unpure vapors containing permanent gases, $\theta_w \neq 1$. The relationship between τ^M and β, obtained by integrating eqn. (7), utilizing eqn. (8):

$$\tau^M = \frac{1}{A-B}\left[\tau_0\ (\beta) + \tau_1\ (\beta, \beta_f^M)\right] \tag{11}$$

where

$$\beta_f^M \equiv \frac{A}{A-B}\ \beta_f^3 - \frac{B}{A-B}\ \frac{1}{G^*} \tag{12}$$

and

$$\tau_1(\beta, \beta_f^M) = \frac{1}{3}\ \frac{(\beta_f^M)^3 - 1/G^*}{(\beta_f^M)^{3/2}}\ \ell\left[\frac{1-\beta^{3/2}}{1+\beta^{3/2}} \cdot \frac{\beta^{3/2} + (\beta_f^M)^{3/2}}{\beta^{3/2} - (\beta_f^M)^{3/2}}\right] \tag{13}$$

At the limit, $A = 1$, $\beta \to 0$, $\delta\theta^M \to 0$, $\beta_f^M \to \beta_f$ and eqn. (11) reduces to the relation between τ and β for a single bubble [4, 5]:

$$\lim_{F \to 0}\ \tau^M = \tau = \tau_0\ (\beta) + \tau_1\ (\beta, \beta_f) \tag{14}$$

where $\tau_1\ (\beta, \beta_f)$ is identical in form with eqn. (13) with β_f replacing β_f^M.

The controlling parameters

A quantitative representation of eqns. (10) and (11) requires the knowledge of the "constants" A and B, or rather U_∞^M and δT^M.

The relative velocity between the rising bubbles and up or down flowing continuous phase is given by

$$U_\infty^M = U_b \pm U_\ell \quad \begin{matrix} + \text{ Counter-current} \\ - \text{ Co-current} \end{matrix} \tag{15}$$

where U_b is the bubbles' rise velocity related to the wall and U_ℓ is the superficial velocity of the continuous phase. Equation (15) is substantiated by the experimental conclusion of Baker and Chao [8] that the relative (gas—liquid) velocity of bubbles with $R > 0.3$ cm are practically independent of the continuous phase velocity.

The relative velocity of a bubble in a bubble swarm as a function of the porosity, or fractional-hold-up ϵ, is given by Marrucci [9]:

$$U_\infty^{\mathrm{M}} = U_\infty \frac{(1-\epsilon)^2}{1-\epsilon^{5/3}} \tag{16}$$

where, with the column height $H = t_f U_b = (1/F)(N-1)U_b$

$$\epsilon = \frac{S\, n(4\pi/3) \sum_{i+1}^{N} R_i^3}{S\, H} = \frac{n(4\pi/3) \sum_{i+1}^{N} R_i^3}{(1/F)\, U_b\, (N-1)} \tag{17}$$

Obviously, the correct value of ϵ requires the knowledge R_i, U_b, F and N (or t_f), *i.e.*, the complete collapse history. Hence, the utilization of eqn. (16) requires an iterative procedure (coupled with an "external" iteration (see below) which yields the R_i values). However, for a given iteration eqn. (17) reduces to $\epsilon = C/U_b$, where C = const. Combining (15) to (17) yields

$$U_\infty\, \epsilon(1-\epsilon)^2 - (1-\epsilon^{5/3})\ \ (C \pm \epsilon U_\ell) = 0 \qquad \begin{matrix} + \text{ Counter-current} \\ - \text{ Co-current} \end{matrix} \tag{18}$$

which is solved for ϵ at any iteration. The correct ϵ is the one which corresponds to true values of R_i.

The fractional temperature decrease, $\delta\theta^{\mathrm{M}}$. Consider a periodic operation. During the time interval $\Delta t\ (= 1/F)$ the successive bubbles move within the (assumed) well mixed thermal field, left behind the preceding bubbles, which is at a temperature $T^{\mathrm{M}}_{\infty,i}$, corresponding to $\delta T_i^{\mathrm{M}} \equiv (T^{\mathrm{M}}_{\infty,i} - T_\infty)$. We evaluate the temperature along the bubbles' path in $(N-1)$ discrete sections, each (U_b/F) high. The energy balance on section i yields:

$$U_\ell \rho_\ell C_{p\ell}\, (\delta T^{\mathrm{M}}_{i+1} - \delta T^{\mathrm{M}}_i) = \pm\, nF\, \rho_v\ \lambda(R^3_{i+1} - R^3_i)\,(4\pi/3) \tag{19}$$

where, *counting i downwards*, $\delta T^{\mathrm{M}}_{i+1}$ is the temperature of the continuous phase leaving section 1, related to T_∞, and $\delta T^{\mathrm{M}}_{i+1} = T^{\mathrm{M}}_{i+1} - T^{\mathrm{M}}_i$.

In dimensionless terms, eqn. (19) becomes:

$$\delta\theta^{\mathrm{M}}_{i+1} = \delta\theta^{\mathrm{M}}_i \pm \frac{Q_{v\ell}}{\mathrm{Ja}}\,(\beta^3_{i+1} - \beta^3_i) \tag{20}$$

where $Q_{v\ell}$ is the volumetric ratio of the vapor to liquid flow rate. Note that an energy balance over the whole column yields [1]:

$$\delta\theta^{\mathrm{M}}_0 = \frac{T_{\mathrm{out}} - T_\infty}{T^\star - T_\infty} = \frac{Q_{v\ell}}{\mathrm{Ja}}\ (1-\beta_f{}^3) \tag{21}$$

The collapse history

The collapse history, β *vs.* τ, can be solved analytically from eqn. (11) by approximating A and B by averaging the characteristic parameters over the whole column [1]. A more accurate result is obtained by evaluating $\delta\theta_i^{\mathrm{M}}$ and R_i locally, along the bubbles paths.

The average collapse rate in section i is obtained from eqn. (4):

$$-\dot{\beta}_{i,\mathrm{ave}}^{\mathrm{M}} = \left(\frac{K_{\mathrm{v}}}{\pi}\right)^{1/2} (U_{\infty}^{\mathrm{M}}/U_{\infty})^{1/2} \left[(\theta_{\mathrm{w,ave}} - \delta\theta_{i,i+1}^{\mathrm{M}})\right] \beta_{i,\mathrm{ave}}^{-1/2} \tag{22}$$

where

$$\dot{\beta}_{i,\mathrm{ave}}^{\mathrm{M}} = (\beta_{i+1} - \beta_i)/\Delta\tau \; ; \quad \Delta\tau = \mathrm{Ja}\,\mathrm{Pe}^{1/2}\,(\alpha/R_0^2)\;\; (1/F)$$

$$\beta_{i,\mathrm{ave}} = (\beta_i + \beta_{i+1})/2 \quad ; \quad \theta_{i,i+1}^{\mathrm{M}} = (\delta\theta_{i+1}^{\mathrm{M}} + \delta\theta_i^{\mathrm{M}})/2$$

and

$$\theta_{\mathrm{w,ave}} = (\theta_{\mathrm{w},i} + \theta_{\mathrm{w},i+1})/2$$

evaluated for β_i and β_{i+1} by eqn. (8).

The value of β_{i+1} is obtained by solving eqn. (22), now written as:

$$(\beta_{i+1} - \beta_i)\;\; (\beta_{i+1} + \beta_i)^{1/2} \pm C_1\,(\beta_{i+1}^3 - \beta_i^3) - C_2 = 0 \tag{23}$$

where

$$C_1 = (K_{\mathrm{v}}A/2\pi)^{1/2}\, Q_{\mathrm{v}\ell}\, \Delta\tau/\mathrm{Ja} \; ; \quad C_2 = (2K_{\mathrm{v}}A/\pi)^{1/2}\,(\theta_{\mathrm{w,ave}} - \delta\theta_i^{\mathrm{M}})\,\Delta\tau$$

The solution for β_{i+1} in eqn. (23) requires the knowledge of the parameters for the i section. Knowing R_0 and R_{f} (or β_{f}), we can start the calculation from the top downwards in the counter-current case where T_{∞}^{M} is known ($\delta T_{\infty}^{\mathrm{M}} = 0$). Similarly in the co-current case, we can start from the bottom upwards, since T_{∞}^{M} is known ($\delta T_{\infty}^{\mathrm{M}} = 0$), or from the top downwards, if one utilizes δT_0^{M} (or $\delta\theta_0^{\mathrm{M}}$) the outlet temperature, calculated by eqn. (21). The latter approach allows to utilize the same iterative procedure for the two cases.

Starting with $\beta_{i=1} = \beta_{\mathrm{f}}$ counting downwards, ($\delta\theta_1 = 0$ for counter-current flow and $\delta\theta_1 = \delta\theta_0$ for co-current flow) the "internal" procedure for the solution of β_{i+1} for a given ΔT^* proceeds as follows:

(a) Assume a first approximation for β_{i+1} ($= \beta_2^{(1)}$); (b) using $\beta_2^{(1)}$, calculate $\theta_{\mathrm{w,ave}}$ (eqn. 8), C_1 and C_2; (c) solve eqn. (23) for $\beta_{i+1} = \beta_2^{(2)}$; (d) calculate $\theta_{\mathrm{w,ave}}$ C_1, C_2; (e) calculate $\beta_2^{(3)}$ by eqn. (23); (f) continue steps (d) and (e) until $\beta_2^{(\mathrm{m})} = \beta_2^{(\mathrm{m}-1)}$.

The first value of β_{i+1} ($= \beta_2$) is then used to calculate $\delta\theta_{i+1}^{\mathrm{M}}$ by eqn. (20). The above procedure is then repeated to evaluate all β_{i+1} for $(1 < i < N-1)$.

Evaluation of N and $\Delta T^{\star}$. At a given bubble spacing (n and F), the number of bubbles N which constitute the bubble column depends on the temperature driving force. Low N represents small condensation time due to high temperature driving force, while high values of N (at the same n and F) represent low condensation rates. An external procedure for evaluating $\Delta T^{\star}$ for values of N (so that $\beta_N = 1$) was utilized. If $\beta_N \neq 1$, $\Delta T^{\star}$ is corrected and the procedure is started again. Note that U_{∞}^{M} must be calculated for each new value of N, since $U_{\infty}^{M} = f(\epsilon)$ and ϵ varies with N. A summary of the general procedure used to evaluate the effect of the various parameters follows.

Summary of the general procedure. (a) Set n; (b) Set F; (c) Set N, and estimate $\beta_{i+1}^{(1)}$, the initial values of β_{i+1}; (d) Determine U_{∞}^{M} by solving eqn. (18); (e) Assume $\Delta T^{\star}$; (f) Calculate β_{i+1} by eqn. (23) and the above "internal" interaction procedure; (g) Use calculated value of β_{i+1} to calculate δT_{i+1}^{M} by eqn. (20); (h) If $\beta_N \neq 1$ change $\Delta T^{\star}$ and repeat (f); (i) Take new N and repeat stages (d) to (h); (j) Take new F and repeat (c) to (i); (k) Take new n and repeat (b) to (j).

Results and discussion

For ease of comparison with earlier data [1], $R_0 = 0.25$ cm is retained in all runs considered here.

Figure 1 represents the velocity ratio $U_{\infty}^{M}/U_{\infty} = A^2$ as a function of bubble frequency at different horizontal spacings. Note that $n = 4$ nozzles per cm^2 corresponds to a packed layer in which the bubbles touch each other. As is to be expected, A decreases as bubble density (F and/or n) increases. The effect of non-condensables in the bubbles on the velocity ratio is comparatively small, and is not shown here. For a given F and n, A was found to be independent of $\Delta T^{\star}$, or the condensation rates, except at very low (up to 0.5°C) $\Delta T^{\star}$'s. At these small driving forces the value of A decreases with $\Delta T^{\star}$ due to relatively high value of ϵ (low condensation rate). At identical F and n, the value of A is larger for co-current flow than for counter-current flow. This is due to the fact that in the parallel flow case the condensation rate is highest at the inlet where the bubbles are the largest. This strongly affects the vapor hold-up resulting with a decrease of the average value of ϵ and a moderate increase of A as compared with the counter-current case. Similar results were obtained for the two-component pentane—water system.

Figure 2 represents the dimensionless temperature driving force profile in the column, along the bubbles path. Naturally, the liquid temperature increases (in the liquid flow direction), as bubble density (F and n) increases. Note that θ_w (wall temperature of a single bubble) is identical for the two flow configurations, but $\theta_w^{M} = \theta_w - \delta\theta^{M}$ varies appreciably. Whereas in the counter-current case $\delta\theta^{M}$ has its maximum value at the bottom of the column, $\delta\theta^{M}$ is maximum at the top of the column in co-current flow. For a pure vapor bubble $\theta_w = 1$, $\theta_w^{M} > 0$, and condensation is unhalted. In the

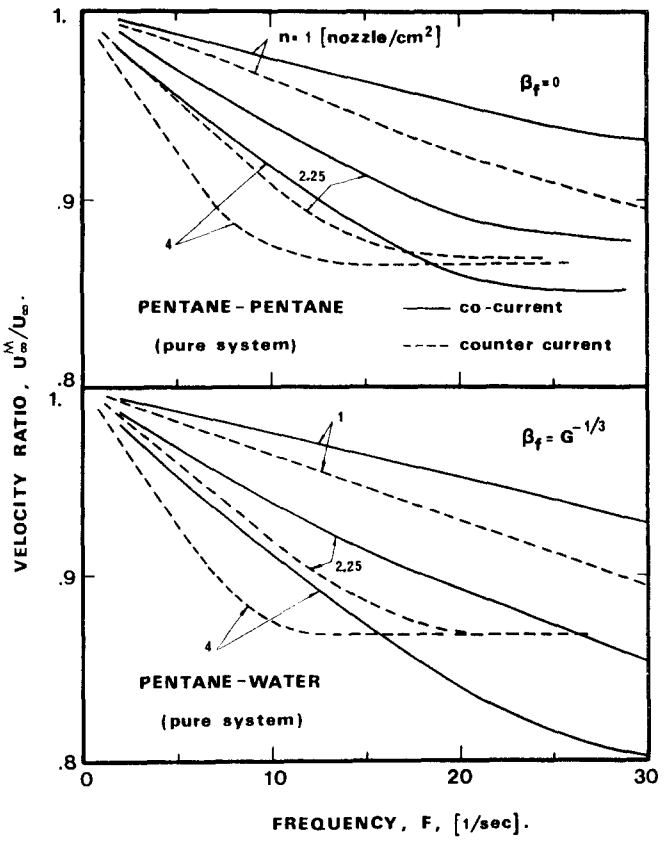

Fig. 1. Velocity decrease due to bubble density.

presence of inerts, θ_w decreases as condensation proceeds. θ_w and $\delta\theta^M$ decrease upwards in the column in counter-current flow, and θ_w^M is usually positive. However, in parallel flow θ_w decreases while $\delta\theta^M$ increases (upwards) and θ_w^M may approach zero, thus halting the condensation process. As seen in Fig. 2, condensation is stopped in the co-current case while, at the same ΔT^*, it proceeds to completion in the counter-current case. Similar results were obtained with the pentane—water system.

Figure 3 represents $(A-B) = A(1-\delta\theta_{ave}^M)$ as a function of the nominal driving force, ΔT^*, for various operating conditions. Note that for pure vapors $A - B = \tau_0/\tau_0^M$, *i.e.* the ratio of single bubble to multi-bubble condensation times corresponding to the same β. As seen by eqn. (11), this relationship does not hold in the presence of non-condensables. As seen in Fig. 3, $(A - B)$ decreases with bubble density. For the same F, $(A - B)$ decreases as n increases. These results are at variance with those obtained for a single bubble-train in an infinite expanse where $(A - B)$ approaches unity as F increases [3]. This is due to the fact that frequency in a single train effects

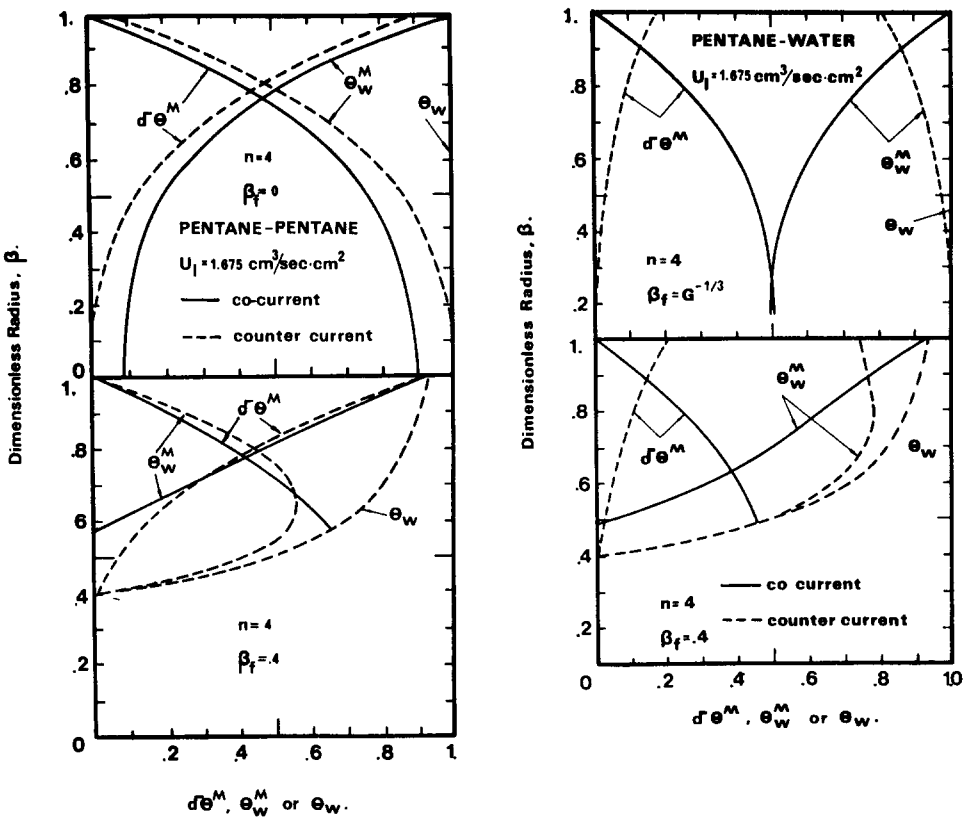

Fig. 2. Temperature decrease, bubble wall temperature and temperature driving force along the column.

an increase in the rise velocity, thus enhancing condensation through stronger convection effects. Here, however, the rise velocity decreases as ϵ increases. For comparable conditions, the decrease of $(A - B)$ with F and/or n is more pronounced in the co-current flow case, indicating a larger condensation time in this case.

As seen in Fig. 4, $(A - B)$ increases as the continuous flow rate is increased and the condensation rate increases accordingly. As expected, this effect is much more pronounced in the co-current flow system.

The dimensionless bubble collapse history is presented in Fig. 5. The collapse rate decreases as the spatial density of the bubbles increases [1]. This effect is more pronounced in the single-component system, consistent with the corresponding $\delta\theta^M$ values exhibited by this system, as compared with those of the two-component (pentane—water) system. This is due to the difference in the volumetric heat capacities of the two continuous phases.

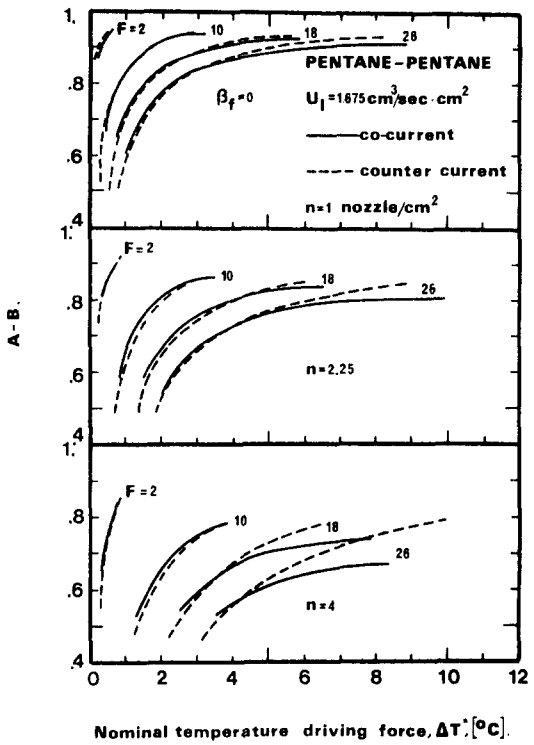

Fig. 3a. Effects of frequency and horizontal bubble spacing on $A - B$ as a function of nominal driving force.

The collapse history of a single bubble in an infinite constant temperature expanse is also included in Fig. 5 for comparison.

Consistent with the results shown in Fig. 2, the $\beta - \tau$ relationship varies for the two flow configurations: initial condensation rate in the co-current case is higher than in the counter-current case (higher θ_w^M). However, the condensation rate in the co-current case decreases fast and, in the presence of inerts, may even come to an end without reaching the final possible size. (In this case $C_2 = 0$ in eqn. 23.) Again, due to the difference in the volumetric heat capacities, the pentane—water system is less affected by the flow direction than the pentane—pentane system.

Figure 6 represents the column height required for condensation of 99% of volume of the vapor that can condense at the given operating conditions. In general, the closer the horizontal and/or vertical bubble spacing, at identical nominal temperature driving forces, the higher the column required. This effect is particularly noted at low temperature driving forces and, consistent with single-train studies, is much more pronounced in the presence of inerts.

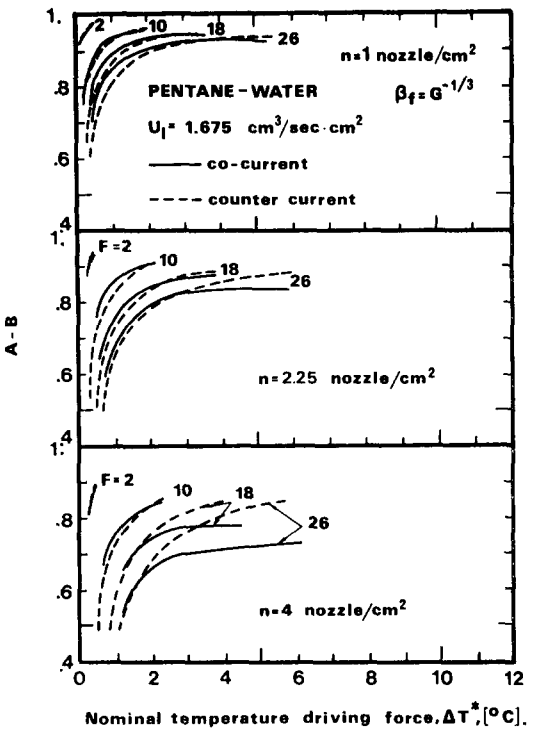

Fig. 3b. Effects of frequency and horizontal bubble spacing on $A - B$, as function of nominal driving force.

For a given n, flow rate and inlet continuous phase temperature T_∞, the frequency (*i.e.* the vapor flow rate) determines the temperature driving force along the column. The asymptotic minimum possible $\Delta T^\star$ noted in Fig. 6 corresponds to $\theta_w^M \to 0$ and represents the minimum nominal $\Delta T^\star$ which may still yield complete condensation. The asymptotic value of $\Delta T^\star$ increases with n and F, *i.e.* the dispersed phase flow rate. Since the change in the temperature driving force depends on the volumetric specific heat, the pentane—pentane system should be more sensitive to change in F and n than the pentane—water system. This is evident from the curves for the single- and two-component systems. The effect of the counter-current continuous-phase flow is to decrease the column height even below that required for a single bubble in a quiescent infinite medium. This is particularly noted at low bubble densities of pure systems, where the apparent height for the multi-bubble column is lower than that of a single bubble. The effect is reversed in the co-current flow case. This is easily understood by realizing that the collapse rate is determined by the relative velocity U_∞^M while the column height is evaluated by reference to the bubbles' velocity relative to the wall, U_b =

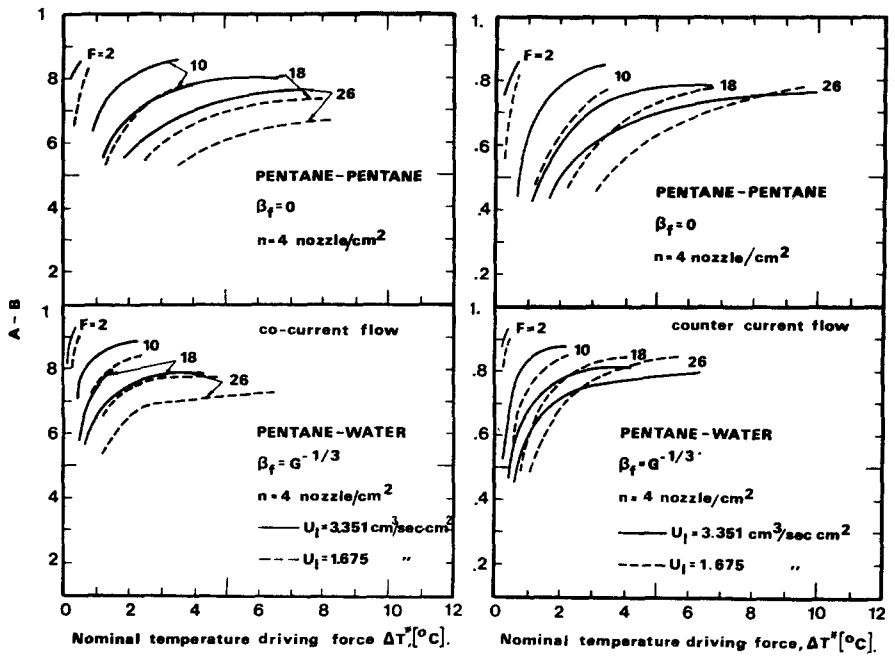

Fig. 4. Effect of the continuous phase flow rate on $A-B$.

$U_\infty^M \mp U_\ell$). For a single bubble in a still column $U_b = U_\infty$. The condensation height ratio (multi to single bubble) is given by

$$\frac{H^M}{H} = \frac{(U_\infty^M \mp U_\ell)t_f^M}{U \cdot t_f} = \frac{\tau_f^M}{\tau_f}\left(A^2 \mp \frac{U_\ell}{U_\infty}\right) \quad \begin{matrix} - \text{ counter-current} \\ + \text{ co-current} \end{matrix} \tag{24}$$

For low bubble density the values of A and τ^M/τ are close to unity, and the condensation height ratio will strongly depend on U_ℓ, the continuous phase (superficial) velocity.

The instantaneous interfacial heat transfer coefficient for the multi-bubble system is defined by $h^M = q^M/s\,\Delta T_w^M$ where q^M, s and ΔT_w^M are the instantaneous heat flux, surface area and temperature driving force, respectively. For identical values of β, eqns. (1), (3) and (4) yield: $q^M/q = \beta^M/\beta = (\theta_w^M/\theta_w)A$ and:

$$\frac{h^M}{h} = A = (U_\infty^M/U_\infty)^{1/2} \tag{25}$$

Thus, one can easily determine h^M by utilizing eqn. (1) and Fig. 1. More useful information is gained by defining the volumetric heat transfer

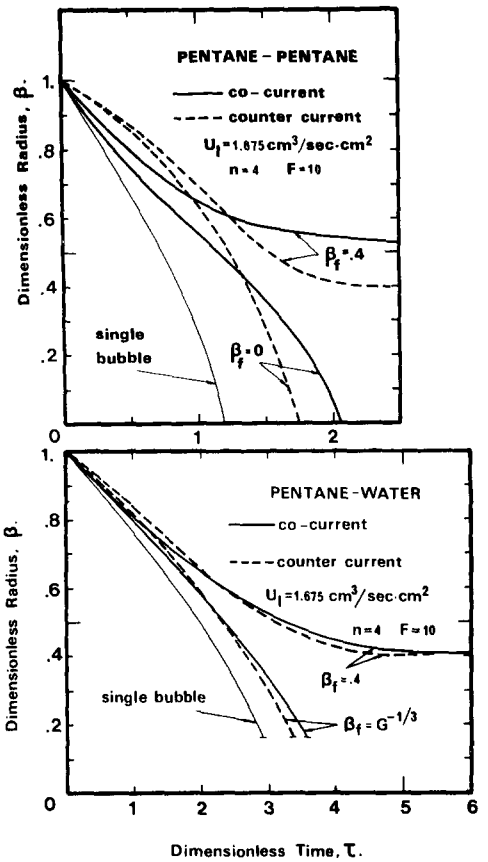

Fig. 5. Collapse history in multi-bubble system compared with single-bubble system.

coefficient

$$U_v = \frac{Q/t_f}{V \cdot \Delta T_{ave}} \tag{26}$$

where Q/t_f represents the average heat flow rate, V denotes the optimal volume (based on height for complete condensation as defined above) and ΔT_{ave} is the (arithmetic) average temperature driving force along the column. Figure 7 represents the calculated values of U_v which are plotted, for ease of reference, against the nominal driving force. In general, the volumetric transfer coefficient in co-current flow is lower than in the counter-current flow case and, in both configurations, increases with increasing the dispersed phase flow rate (F and n), consistent with earlier spray column studies of evaporating drops [10, 11]. As already noted in our single bubble studies [7], the pentane—water system exhibits transfer coefficients which are some 50% above those of the pentane—pentane system. This is due to the higher heat capacity and thermal conductivity of water as compared to pentane. The

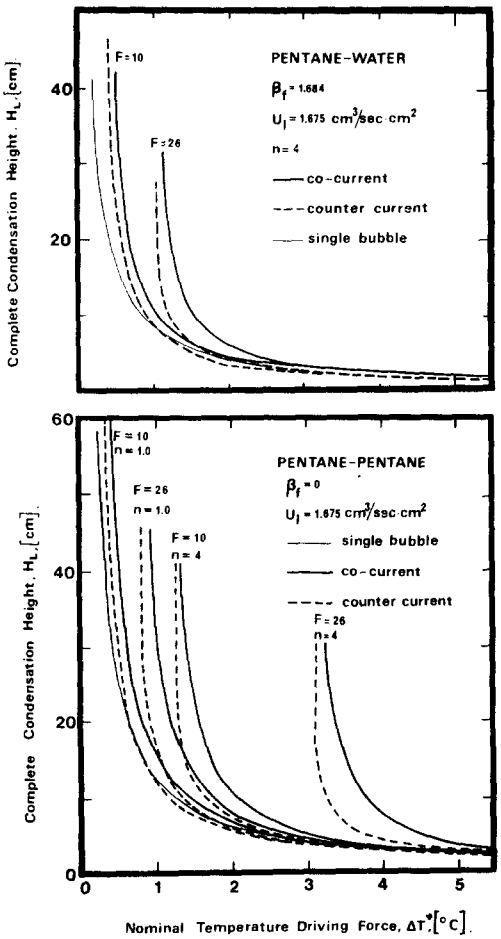

Fig. 6. Effect of bubble density on the complete condensation height.

superficial vapor velocities considered here, 0.63 cm^3/sec cm^2 to 6.5 cm^3/sec cm^2, were kept low, so as to maintain the identity of each bubble. In this sense, this study is limited to the "streamline" flow region, where (for air–water system) the hold-up is linearly proportional to the dispersed flow rate. Here, however, the dispersed phase hold-up decreases due to condensation as the bubbles rise along the column.

The numerical values for the overall heat transfer coefficients are in general agreement with those realized in these laboratories and others reported in the literature.

The values of U_v range from 1.6×10^3 kcal/h m^3 °C [$\simeq 10^2$ BTU/h ft^3 °F] at low F and n to 4.3×10^5 kcal/h m^3 °C [$\simeq 2.7 \times 10^4$ BTU/h ft^3 °F] at n = 4 and F = 26. Direct-contact condensation in a venturi mixed co-current pipe flow of steam in Aroclor yielded values in the range of 1.5×10^5 to 4×10^5

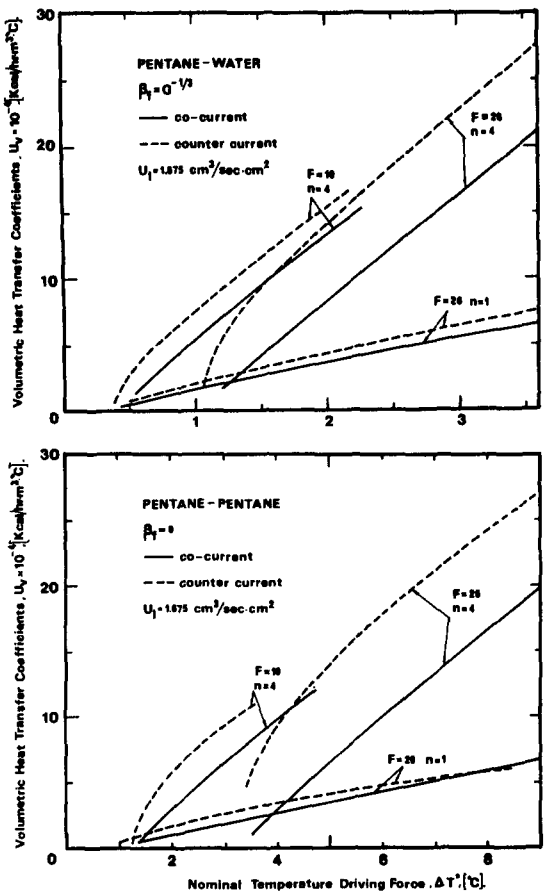

Fig. 7. Overall volumetric heat transfer coefficients at various operating conditions. Pure pentane—pentane system.

BTU/h ft^3 °F [12]. Order of magnitude smaller values were reported when a co-current spray column was used [12, 13]. Values up to 4×10^5 BTU/h ft^3 °F were reported by Harriott and Wiegandt [14] for a co-current, turbulent, downflow sieve plate condenser. However, these values were arbitrarily based on the exit temperature driving force and a 3-in. height. Condensation of methyl chloride in water in co-current flow through a packed bed yielded U_V between 6.5×10^4 and 1.5×10^5 BTU/h ft^3 °F [14], Wilke *et al.* [13] reported U_V of about 6×10^3 BTU/h ft^3 °F for steam condensing in Aroclor in a counter-current packed bed. Again, meaningful comparison is difficult since arbitrary values were used for column heights.

Conclusions

(1) An analysis of the collapse history of a multi-bubble system in the

streamline region was obtained by assuming quasi-steady state and solving for the local driving forces along the bubble column. The solution makes it possible to evaluate the independent effects of bubble frequency F, horizontal spacing n and inerts contents in single- and two-component systems, in either co-current or counter-current flow.

(2) Single bubble studies may not be used to design multi-bubble systems, since interaction effects are pronounced and should not be neglected. However, a multi-bubble system may be analyzed by treating a representative single bubble, provided that the correct flow and temperature fields, which account for bubble density, are used.

(3) The effect of the horizontal bubble spacing is much more pronounced than that of the vertical one.

(4) Counter-current is more efficient than co-current operation. Complete condensation in the presence of non-condensable inerts can only be achieved by utilizing a counter-current flow exchanger.

Nomenclature

A	velocity ratio $(U_\infty^{\mathrm{M}}/U_\infty)^{1/2}$
B	operational variable
C, C_1, C_2	constants
$C_{p\ell}$	heat capacity continuous phase
F	bubble frequency
Fo	Fourier number $(\alpha t/R_0^2)$
$G^\star$	density ratio volatile fluid $(\rho_{\mathrm{L}}/\rho_{\mathrm{v}})$
H	condensation height
h	instantaneous transfer coefficient
i	index of a bubble in a row
Ja	Jakob number $C_{p\ell}\ (T^\star - T_\infty)/\lambda\rho_{\mathrm{v}}$
K	constant $(K_{\mathrm{v}}/\pi)^{1/2}$
K_{v}	velocity factor
k	thermal conductivity, continuous phase
N	number of bubbles in a row
n	nozzles per unit area
Pe	Peclet number $(= 2 R_0\ U_\infty/\alpha)$
$Q_{v\ell}$	flow rate ratio, vapor to liquid
q	instantaneous heat flux
R	instantaneous radius of bubble
R_0	initial radius of bubble
R_{f}	final condensation radius
$\dot{R}$	radial velocity $(\mathrm{d}R/\mathrm{d}t)$
S	cross-section area of column
s	surface area of bubbles
T	temperature
T_{out}	outlet temperature, continuous phase

T_w	bubble wall temperature
T^*	saturation temperature at pressure of the system
T_∞	approach (inlet) temp., continuous phase
T_∞^M	local temperature of continuous phase
ΔT_w	temperature driving force $(T_w - T_\infty)$
ΔT^*	temperature driving force $(T^* - T_\infty)$
δT^M	local temperature increase $(T_\infty^M - T_\infty)$
δT_0^M	overall temperature increase $(T_{out} - T_\infty)$
t	time
t_f	time, final condensation
U_b	bubble velocity, relative to wall
U_ℓ	superficial velocity of liquid (Q_ℓ/S)
U_∞	velocity, single bubble system
U_∞^M	multi-bubble velocity, relative to liquid
U_v	volumetric heat transfer coefficient
V	optimal column volume
Y_0	initial concentration of inerts
α	thermal diffusivity, continuous phase
β	dimensionless radius (R/R_0)
β_f	final dimensionless radius (R_f/R_0)
λ	latent heat
θ	dimensionless temp. $(T - T_\infty)/(T^* - T_\infty)$
θ_w	dimensionless temp. $(T_w - T_\infty)/(T^* - T_\infty)$
θ_w^M	dimensionless temp. driving force $((T_w - T_\infty^M)/(T^* - T_\infty))$
$\delta\theta^M$	local temp. decrease $((\delta T^M)/(T^* - T_\infty))$
$\delta\theta_0^M$	overall temp. decrease $((\delta T_0^M)/(T^* - T_\infty))$
ρ	density, continuous phase $(= \rho_\ell)$
ρ_L	density of liquid, dispersed phase
ρ_v	density of vapor, dispersed phase
ϵ	gas hold-up volume fraction
τ	dimensionless time (Ja $Pe^{1/2}$ Fo)
τ_0	dimensionless time, pure vapor
τ_1	dimensionless time, correction due to inerts

References

1 D. Moalem and S. Sideman, in E.U. Schlunder (Ed.), Proc. 5th Seminar Int. Centre Heat Mass Transfer, Trogir, Yugoslavia, 1972, in the press, 1973.

2 D. Moalem, S. Sideman, A. Orell and G. Hetsroni, Direct contact heat transfer with change of phase: condensation of a bubble train, Int. J. Heat Mass Transfer, 16 (1973) 2305.

3 D. Moalem, S. Sideman, A. Orell and G. Hetsroni, Proc. Int. Symp. Two-Phase Systems, Haifa, Israel, 1971, in G. Hetsroni, S. Sideman and J.P. Hartnett (Eds.), Progress in Heat and Mass Transfer, Vol. 6, Pergamon, Oxford, 1972, p. 197.

4 J. Isenberg, D. Moalem and S. Sideman, 4th Int. Heat Transfer Conf., Paris, 1970, Vol. V, 25B.

5 D. Moalem and S. Sideman, Int. J. Heat Mass Transfer, 14 (1971) 2152.
6 M.J. Boussinesq, J. Math. Pures App. Serv., 1 (1905) 310.
7 J. Isenberg and S. Sideman, Int. J. Heat Mass Transfer, 19 (1970) 945.
8 J.L.L. Baker and B.T. Chao, AIChE J., 11 (1965) 268.
9 G. Marrucci, Ind. Eng. Chem. Fund., 4 (1965) 224.
10 S. Sideman and Y. Gat, AIChE J., 12 (1966) 296.
11 S. Sideman, G. Hirsch and Y. Gat, AIChE J., 11 (1965) 1081.
12 D.L. Lackey, M.S. Thesis, Univ. Calif. Berkeley, 1961.
13 C.R. Wilke, C.T. Cheng, V.L. Ledesma and J.W. Porter, Chem. Eng. Progr., 59 (1963) 69.
14 P. Harriott and H.F. Wiegandt, AIChE J., 10 (1964) 755.